

# Shear properties of passive ventricular myocardium

SOCRATES DOKOS, BRUCE H. SMAILL, ALISTAIR A. YOUNG, AND IAN J. LEGRICE

*Department of Physiology, School of Medicine, University of Auckland, Auckland, New Zealand*

Received 9 February 2002; accepted in final form 23 July 2002

**Dokos, Socrates, Bruce H. Smail, Alistair A. Young, and Ian J. LeGrice.** Shear properties of passive ventricular myocardium. *Am J Physiol Heart Circ Physiol* 283: H2650–H2659, 2002; 10.1152/ajpheart.00111.2002.—We examined the shear properties of passive ventricular myocardium in six pig hearts. Samples ( $3 \times 3 \times 3$  mm) were cut from adjacent regions of the lateral left ventricular midwall, with sides aligned with the principal material axes. Four cycles of sinusoidal simple shear (maximum shear displacements of 0.1–0.5) were applied separately to each specimen in two orthogonal directions. Resulting forces along the three axes were measured. Three specimens from each heart were tested in different orientations to cover all six modes of simple shear deformation. Passive myocardium has nonlinear viscoelastic shear properties with reproducible, directionally dependent softening as strain is increased. Shear properties were clearly anisotropic with respect to the three principal material directions: passive ventricular myocardium is least resistant to simple shear displacements imposed in the plane of the myocardial layers and most resistant to shear deformations that produce extension of the myocyte axis. Comparison of results for the six different shear modes suggests that simple shear deformation is resisted by elastic elements aligned with the microstructural axes of the tissue.

mechanical and constitutive properties; anisotropy; strain softening and history; shear testing; laminar structure

VENTRICULAR MYOCARDIUM has a complex architecture in which myocytes are organized in branching layers separated by extensive cleavage planes (13, 26). This laminar structure may be characterized at any point by identifying axes aligned 1) with the myocyte direction, 2) transverse to the myocyte axis within a layer, and 3) normal to the layer. Separate families of perimysial connective tissue are associated with these different material directions (1, 18).

Shear deformation or relative sliding of myocardial layers is thought to play an important role in the mechanical function of the heart. There is evidence that this mechanism facilitates left ventricular (LV) ejection by contributing to subendocardial wall thickening during systole (14). Similarly, the progressive wall thinning that occurs during passive ventricular filling is associated with reorientation or shearing of myocardial layers (21). Emery et al. (5) reported strain softening with LV inflation in the isolated arrested heart and argued that this was caused by shear dis-

placement of adjacent muscle layers and resultant disruption of the perimysial collagen fibers connecting them.

Despite the evident importance of shear deformation in normal ventricular function, little direct information is available about the shear properties of myocardium. Instead, experimental investigation of cardiac material properties has largely been limited to biaxial testing of noncontracting ventricular myocardium in which tensile strains are applied to thin slices of tissue along the myocyte axis (or fiber direction) and transverse to it (3, 10, 20). These studies have demonstrated nonlinear, anisotropic mechanical behavior, with greatest stiffness in the fiber direction. Although it is possible to study in-plane shear properties using biaxial mechanical testing (19), this approach has not been applied to myocardium. It is generally assumed that the material properties of passive ventricular myocardium are determined by the organization of the cardiac connective tissue matrix and are the same in all directions transverse to the fiber axis (i.e., are transversely isotropic). However, the latter assumption is not consistent with the observed structure of ventricular myocardium (13, 26) or with the results of some previous experimental studies (20).

The shear properties of passive ventricular myocardium have been inferred from general constitutive models that incorporate aspects of myocardial architecture together with information derived from biaxial testing (9, 11, 12, 16). The most recent of these (11, 16, 24) are orthotropic constitutive laws that incorporate realistic descriptions of cardiac laminar architecture. However, the validity of such material laws is limited by the fact that they utilize data obtained under tensile loading only, employing thin slices of myocardial tissue in which important structural features have been disrupted.

We report the outcome of a comprehensive experimental investigation of the shear properties of passive ventricular myocardium. To our knowledge, this is the first time that such a study has been carried out. Controlled, simple shear displacement was applied to small cubic samples in which the principal features of myocardial architecture were preserved. Our methods have enabled us to characterize the shear properties of passive ventricular myocardium in relation to its lam-

Address for reprint requests and other correspondence: I. J. LeGrice, Dept. of Physiology, University of Auckland, Private Bag 92019, Auckland, New Zealand (E-mail: i.legrice@auckland.ac.nz).

The costs of publication of this article were defrayed in part by the payment of page charges. The article must therefore be hereby marked "advertisement" in accordance with 18 U.S.C. Section 1734 solely to indicate this fact.

inar structure, providing a more complete material description than has previously been available.

**METHODS**

*Myocardial samples.* All surgical procedures were approved by the Animal Ethics Committee of the University of Auckland. Six pigs (26–32 kg body wt) were anesthetized initially with tiletamine-zolazepam (Zoletil, 10 mg/kg im) and maintained with halothane (2–5%) in oxygen. The heart was exposed via a midsternal thoracotomy, and the animal was heparinized (100 IU/kg). The heart was arrested by rapid injection of 50 ml of cold 15% potassium citrate solution into the LV cavity while the aorta was occluded. It was then excised and placed in cold saline. Then the coronary arteries were cannulated and, within 15 min of excision, perfused with cooled (4°C) cardioplegic solution. The cardioplegic solution consisted of St. Thomas' Hospital no. 1 solution with 50 mM 2,3-butanedione monoxime (BDM), which is known to inhibit cross-bridge activity and prevents contracture arising from cutting injury (15).

After perfusion, the atria were removed and a transmural base-apex segment was cut from the lateral LV wall between anterior and posterior papillary muscles (Fig. 1A). The anterior transmural face was stained with Evans blue dye to highlight the laminar structure. It is possible to define a right-handed orthogonal set of axes at every material point within the ventricular wall on the basis of the local laminar architecture. As shown in Fig. 1A, these axes correspond to the mean myofiber direction (*F*), the direction transverse to the fiber axis within the layer (*S*), and the direction normal to the layers (*N*). A thick section was then cut parallel to the

midwall muscle layers at about one-third of the distance from base to apex (Fig. 1A). A region was selected in which mid-wall muscle layers were most uniform in orientation. Three adjacent cubic blocks measuring  $\sim 3 \times 3 \times 3$  mm were then dissected so that their edges were aligned with the laminae on the transmural face (*S* axis) and with two sides parallel to the *F* and *N* directions (Fig. 1A). For each cubic block, the side facing the apex was then marked with red dye so that the two colored faces could be used to define sample orientation. The blocks were maintained in a chamber containing the cardioplegic solution bubbled with carbogen (95% O<sub>2</sub>-5% CO<sub>2</sub>). The first sample was ready for testing within 60 min of cardiac arrest. With the use of these protocols, shear properties of samples were found to remain unchanged for several hours after arrest in two separate control experiments.

*Shear test device.* The shear test device has been described in detail elsewhere (4). Briefly, samples are attached to the upper and lower platforms of the device and bathed in the cardioplegic solution. The upper platform remains fixed, while the lower platform is moved laterally via a two-dimensional translation stage driven by orthogonal direct-current motors (Physike Instrumente). The device incorporates a triaxial array of force transducers that enables the three-dimensional forces on upper and lower faces of the tissue block to be characterized fully. The Z-force transducer has been modified from its previous description (4) to a subminiature load cell that provides greater force resolution (model 13, RDP Electronics). Shear displacement is measured to submicrometer resolution using magnetic encoders in the direct-current motors. The shear testing system was controlled and data were acquired using a Macintosh 9150/120

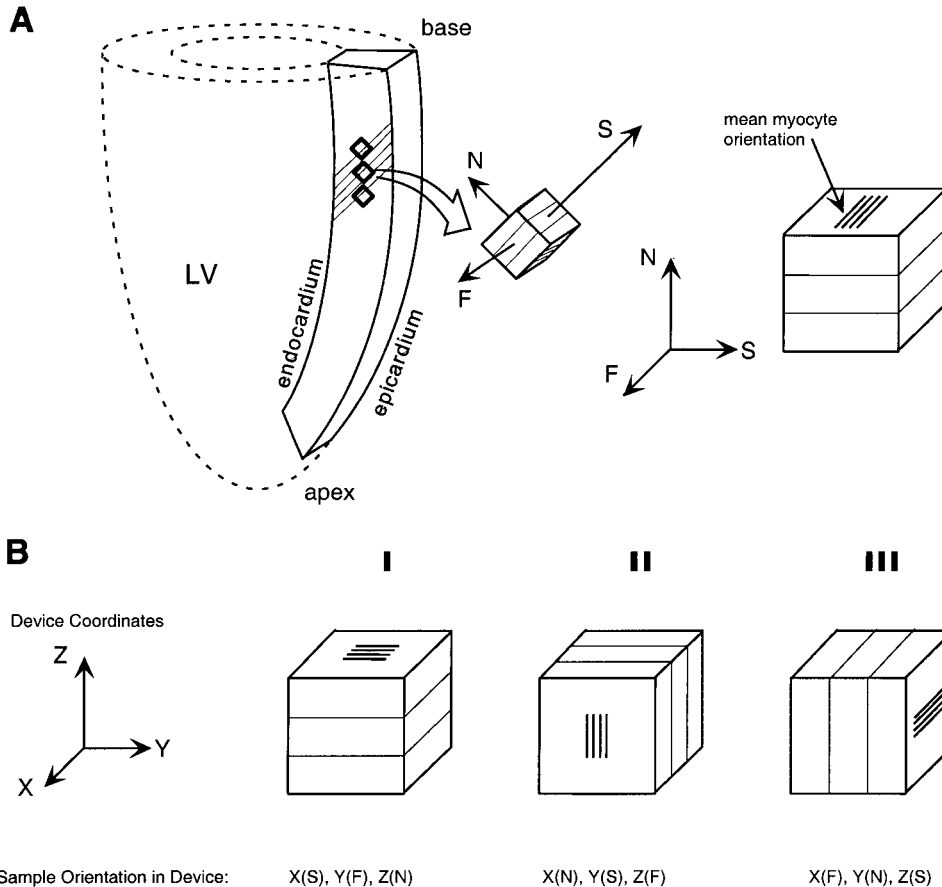


Fig. 1. A: locations and orientation of samples. Schematic represents transmural base-apex segment cut from lateral left ventricular (LV) free wall. For midwall locations, orientation of muscle layers in transmural plane is at  $\sim 45^\circ$  to the base, whereas myocytes have a circumferential orientation and are therefore perpendicular to transmural plane. Orthogonal right-hand coordinate system *FSN* reflects this local architecture: *F* denotes fiber orientation, *S* is transverse to the fiber axis within layers, and *N* is the sheet normal direction. Adjacent cubic blocks  $\sim 3 \times 3 \times 3$  mm were cut so that their edges were aligned with the *FSN* axes. B: 3 possible sample orientations within shear test device (*I*, *II*, and *III*). Shear displacement is imposed by translating lower surface of specimen in *X* or *Y* directions with upper surface fixed.

PowerPC computer equipped with analog interface and timer input/output boards (models NB-MIO-16 and NB-TIO-10, respectively, National Instruments). All instrumentation software was written using the LabView (National Instruments) programming language.

**Shear testing.** Before testing, the dimensions of each myocardial block were measured using a micrometer. Absorbent paper soaked with a small drop of cyanoacrylate adhesive was used to attach the samples to the upper and lower platforms in the device. Proper setting of the glue was ensured by compressing the block between the upper and lower platforms with a load of 400–600 mN. This technique was found to provide a high-strength bond in shear while preventing penetration of the glue into the tissue. After 10 min of compression, the bath was filled with cardioplegic solution, and the interplatform separation was returned to the measured resting height of the tissue. The Z force was monitored during this process to ensure that it returned to within a few millinewtons of zero.

Shear testing was performed under quasistatic conditions. Sinusoidal tests were carried out first. Four cycles of sinusoidal (30-s period) displacement were imposed separately in X and Y directions. A succession of tests was carried out in which maximum displacement was increased through 10, 20, 30, and 40–50% of specimen thickness. The term “shear displacement” refers to a displacement of the top plate relative to the bottom plate. A shear displacement of 10 or 50% gives rise to a corresponding Green strain tensor component of 0.05 or 0.25, respectively. The APPENDIX outlines the relationship between shear displacements, deformation gradients, and components of the Green strain tensor. The order of X and Y tests was varied from sample to sample but remained unchanged for a given sample. Asymmetry of shear properties was commonly observed in initial tests. This was due, in part, to residual shear strain caused by small relative displacements of upper and lower surfaces of the specimen during mounting. Residual shear displacement was estimated from initial test results, and the lower platform was offset to correct for this. In all cases, the offset needed to minimize residual shear displacement was <10% of the sample thickness. On completion of sinusoidal testing, separate step tests were performed in X and Y directions. A rapid 50% shear displacement was imposed, and the resultant forces were recorded for 300 s. These protocols were carried out for all three samples from each heart, with samples mounted in random order, in one of the different orientations (I, II, and III) shown in Fig. 1B. A schematic representation of the six different modes of shear deformation achieved by imposing X and Y shear displacements in the three specimen orientations (I, II, and III) is given in Fig. 2.

On completion of testing, all samples were carefully examined for evidence of penetration of glue into the specimen or along its unattached sides, which could introduce artifacts in measured shear properties. The blocks were then stored in formalin for future morphological analysis. Shear displacement is expressed in dimensionless units (displacement ÷ sample thickness), and shear stress was estimated as shear force ÷ surface area.

**Data analysis.** Values are means ± SE. Comparison of grouped data was made using multiway, repeated-measures analysis of variance.  $P \leq 0.05$  is considered to be significant.

## RESULTS

In all hearts tested, midwall muscle layers were inclined at ~45° to the radial direction. Although it was possible to identify a predominant midwall orientation of myocardial laminae on the transmural cut surfaces, there were commonly regions where layers were oriented at ~90° to this principal direction (Fig. 3). The patterns of intersection were not uniform in the circumferential direction, varying significantly over submillimeter dimensions. When examined with a low-power microscope, 9 of 18 sample blocks tested in 6 hearts showed evidence of planes intersecting at ~90° on ≥1 transmural face. Although the blocks were removed from near the midwall, where fiber angle does not change steeply, the orientation of the sheets as seen on the FN surfaces (which represent the “fiber angle”) was not the same on both of these surfaces (on opposite sides of the block), indicating that there was some change in sheet orientation, up to a maximum of 30°, across each block.

Results from a representative shear test, in which four cycles of sinusoidal shear displacement with an amplitude of 40% were applied in the NF mode, are presented in Fig. 4. The viscoelastic properties of this myocardial specimen are evident in the stress-strain hysteresis and in the stress relaxation behavior after 50% step shear displacement (Fig. 4, inset). Corresponding viscoelastic behavior was observed in all specimens.

In sinusoidal tests, stress was always greater on initial displacement in positive and negative directions than in subsequent cycles. After the first cycle, stress-strain loops were reproducible (Fig. 4). This softening

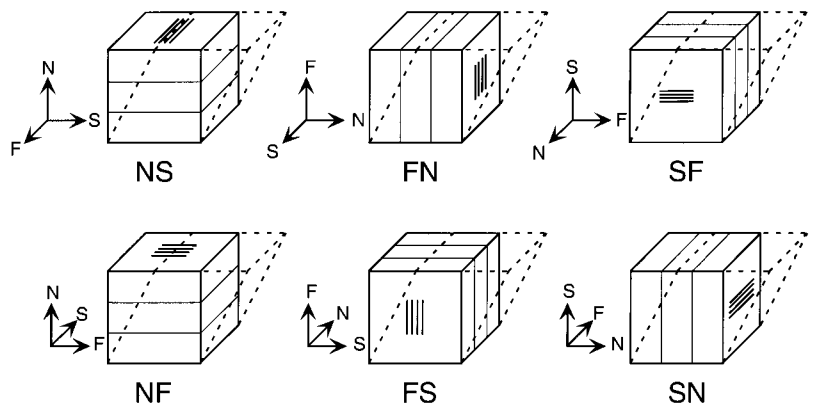


Fig. 2. Six possible modes of simple shear defined with respect to FSN material coordinates. Shear deformation is commonly characterized by specifying 2 coordinate axes: the first denotes (is normal to) the face that is translated by the shear, and the second is the direction in which that face is shifted. Thus NS shear represents translation of the N face in the S direction.

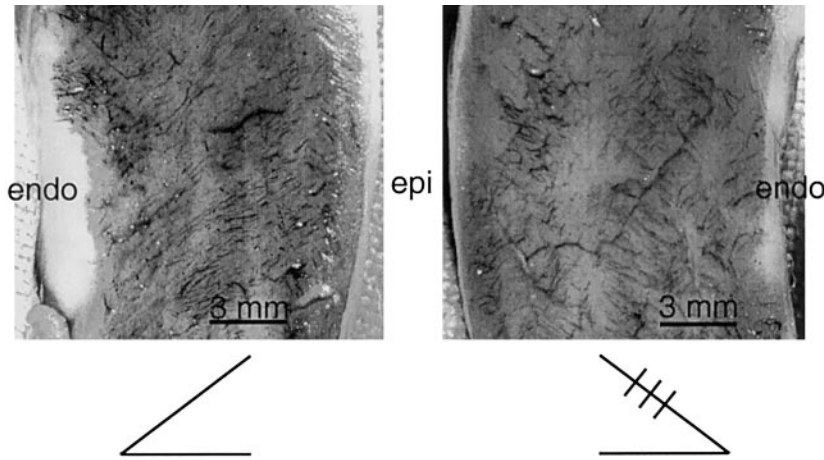


Fig. 3. Laminar arrangement in region of LV free wall from which samples were obtained. Anterior and posterior views of transmural base-apex segment cut from LV lateral free wall of a typical pig heart at the level indicated in Fig. 1A. Both surfaces are coated thinly with Evans blue to highlight cleavage planes between muscle layers. *Left*: muscle layers are relatively uniform and aligned at 45° to base. *Right*: corresponding mirror-image orientation, but intersecting cleavage planes are also evident. Scale bar, 3 mm (typical edge size of tissue blocks).

behavior appears to be inelastic and strain history dependent. In preliminary control experiments, there was no recovery of high initial stresses when test protocols were repeated after the specimen was maintained in an unloaded state for 1 h. Equivalent softening was seen in the *Y* direction after testing in the *X* direction and vice versa. Strain softening was observed at all amplitudes of shear displacement (at displacements of as little as 2.5% in preliminary experiments). As shear amplitude was increased, the stress-strain curve for the first loading cycle of the new test always followed the conditioned loading curve from the preceding test before relaxing to a new stable state (Fig. 5A). For a given shear amplitude, the relative extent of softening was equivalent in each of the six modes of deformation, despite the fact that associated shear stresses varied by up to an order of magnitude (cf. Figs. 4 and 5A).

Figure 5B illustrates the final cycles of a series of tests performed in *FS* shear mode from *experiment 2*, with shear amplitudes increasing in steps of 0.1 up to a final value of 0.5. Stress-strain loops for tests at

increasing shear strain amplitudes did not overlay each other. As the maximum shear deformation experienced by the tissue increases, the stress for any value of shear strain decreases. Similar effects are seen for the *NS* mode, but with much reduced stress amplitudes for the same deformations (Fig. 5C).

To make meaningful comparison between shear properties of ventricular myocardium in different modes of deformation, specimens must have the same strain history. For this reason, all three blocks from each heart were exposed to matching sequences of shear testing. Figure 6 presents results for all six modes of simple shear (*FS*, *FN*, *SF*, *SN*, *NF*, and *NS*) for three adjacent specimens from a single animal, each exposed to a maximum shear displacement of 0.5 in two directions. The *FN* and *FS* modes exhibited markedly higher shear stresses at equivalent strain than the four other modes, and this was observed in all experiments. Summary data for all six hearts are presented in Figs. 7 and 8. Peak-to-peak stress values for each shear amplitude were averaged, and mean values for all hearts are plotted for each shear direction in Fig. 7. Although the standard errors indicate some variation in absolute values of peak-to-peak stress between hearts, differences between modes of deformation were consistent between experiments. Analysis of the peak-to-peak shear stress data indicates that the shear properties of passive ventricular myocardium are significantly anisotropic, with resistance to shear least in *NS* and *NF* deformation modes, intermediate in *SF* and *SN* modes, and highest in *FN* and *FS* modes. Post hoc trend analysis indicated a significant difference in the relationship between maximum stress and maximum strain for all three pairs of directions, i.e., *NF* and *NS* were different from *SF* and *SN*, which were different from *FS* and *FN* ( $P < 0.05$  in each case, see Fig. 7 legend). However, no difference was observed within pairs; i.e., *NF* was not significantly different from *NS*.

To examine whether there were also significant differences in the limiting shear strains of each mode, a simple three-parameter curve was fitted to the midline data for each test (the mean between the loading and

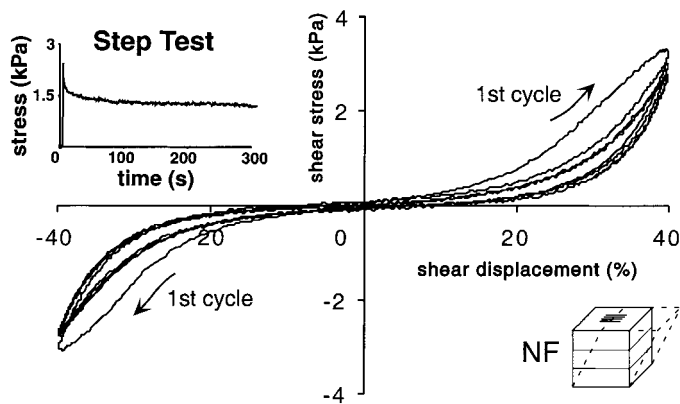


Fig. 4. Relationship between stress and displacement during 4 cycles of sinusoidal simple shear displacement in *NF* mode for typical myocardial specimen shows nonlinear viscoelastic material properties. Maximum displacement is 0.4. Comparable softening occurs during initial displacement in positive and negative directions. *Inset*: stress as a function of time for a simple shear displacement step of 0.5 in *NF* mode.

unloading arms at each value of shear). The form of the curve was

$$\sigma = a \sinh b(x - x_0)$$

where  $\sigma$  is the shear stress (relative to undeformed top surface area of the sample),  $x$  is the shear displacement,  $a$  and  $b$  are parameters defining the shape of the two symmetrical arms of the curve, and  $x_0$  is the displacement offset necessary to account for any asym-

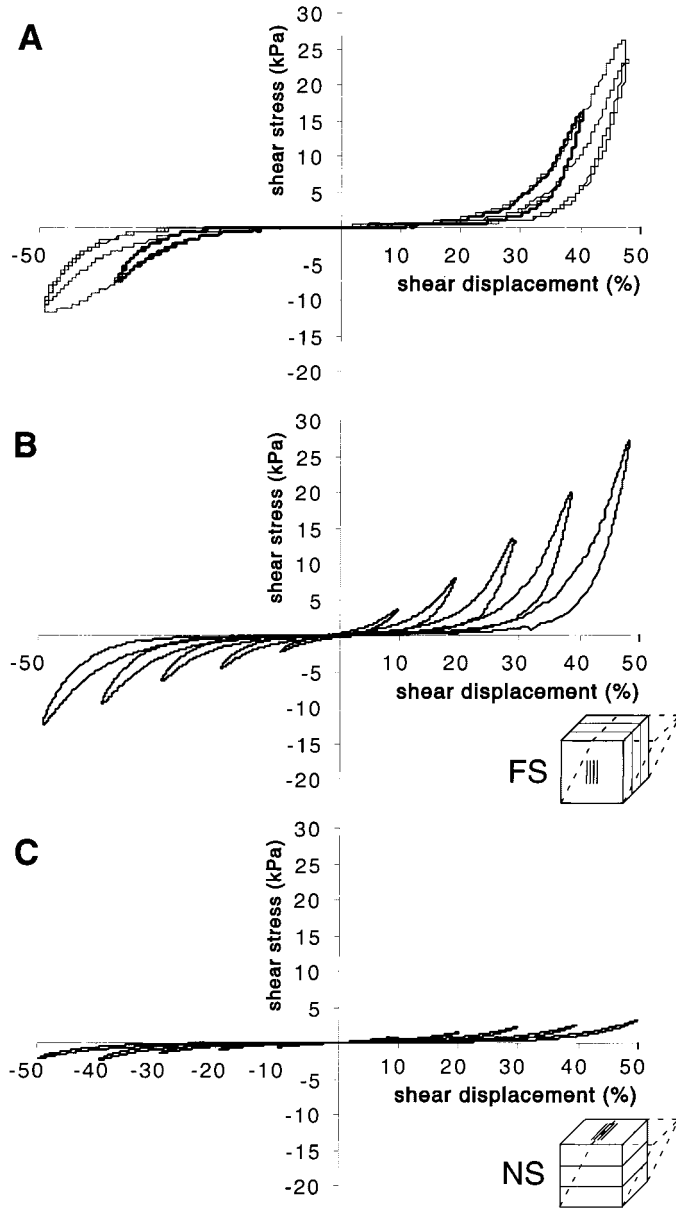


Fig. 5. History dependence of strain softening. *A*: comparison of final 3 cycles of simple shear displacement in *FS* mode at a maximum displacement of 0.4 with all 4 cycles at a maximum displacement of 0.5. First cycle for an increased maximum extension initially follows conditioned curve from preceding test. *B* and *C*: relationship between stress and displacement during final cycles of sinusoidal simple shear displacement for typical myocardial specimens from 1 animal in *FS* and *NS* modes, respectively. Data illustrate history dependence of strain softening. In *B* and *C*, maximum displacement is progressively increased from 0.1 to 0.5.

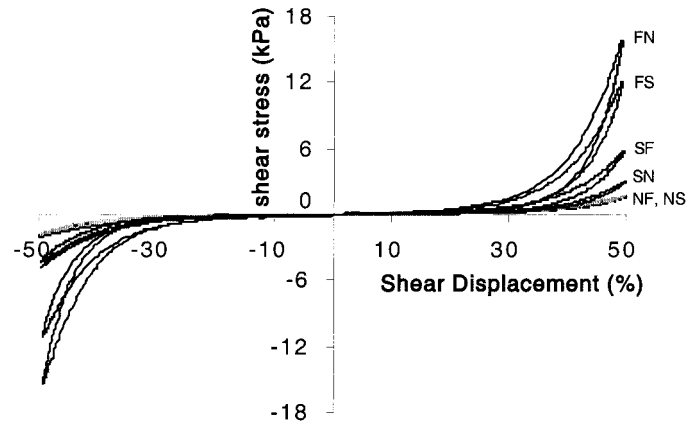


Fig. 6. Relationship between stress and displacement during final cycles of sinusoidal simple shear displacement for typical myocardial specimens from 1 animal in all 6 modes of simple shear displacement. Maximum displacement is 0.5 in all cases. Data show anisotropy of observed material properties with apparent separation between *FN* and *FS*, *SF* and *SN*, and *NF* and *NS* modes.

metry in the data. Limiting behavior is represented by the maximum slope of these fitted curves. Slopes at maximum strain were compared using linear trend analysis. The results were consistent with those outlined above; i.e., *NF* and *NS* were statistically different from *SF* and *SN*, which were statistically different from *FS* and *FN*.

Mean fitted midline curves were also calculated for each maximum displacement and shear direction across all hearts studied. Mean curves for each of the six shear directions at maximum displacements of 0.1, 0.3, and 0.5 are shown overlaid in Fig. 8, illustrating shear anisotropy and strain softening. The mean behavior for the maximum shear displacement of 0.1 is shown on an expanded scale in Fig. 9 (*bottom left*) and indicates a separation of mechanical properties with shear direction at deformations well within the physiological range.

DISCUSSION

This work was motivated by two previous studies. The first (13) demonstrated that ventricular myocardium has a laminar architecture in which myocytes are arranged in distinct layers. The second (14) suggested that shearing of adjacent muscle layers in the inner LV wall contributes substantially to subendocardial wall thickening during systole. The principal aims of the present study were to characterize the shear behavior of passive ventricular myocardium and to determine the extent to which this material behavior reflects the anisotropic structure of the heart wall.

To the best of our knowledge, this work represents the first three-dimensional measurement of myocardial material stiffness aligned with the orthogonal material axes. Our work has shown that the shear properties of passive ventricular myocardium are nonlinear, viscoelastic, and clearly dependent on local myocardial

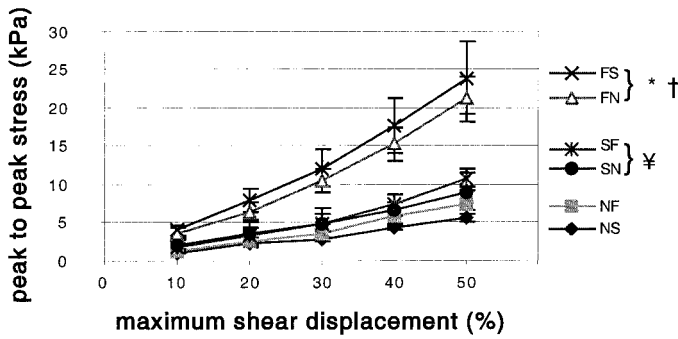


Fig. 7. Change in steady-state (softened) peak-to-peak stresses with increasing maximum simple shear displacements. Data for all 6 simple shear modes were obtained from final cycle of displacement, and maximum displacement was progressively increased from 0.1 to 0.5. Values are means  $\pm$  SE for all 6 hearts tested. Change in peak-to-peak stress with increasing maximum shear displacement is greatest for *FN* and *FS* modes, least for *NF* and *NS* modes, and significantly greater for *SF* and *SN* modes than for *NF* and *NS* modes. However, there was no difference within these pairs. \* $P < 0.05$ , *FN* and *FS*  $>$  *SN* and *SF*; † $P < 0.05$ , *FN* and *FS*  $>$  *NF* and *NS*; ¥ $P < 0.05$ , *SN* and *SF*  $>$  *NF* and *NS*.

architecture. Moreover, the study produced three further novel results. First, passive ventricular myocardium exhibited strain softening throughout and beyond the physiological range of shear deformation. Second, passive ventricular tissue appears to be markedly resistant to simple shear deformations that produce extension of the myocyte axis. Third, stiffness along these axes increases in the following sequence:  $N < S < F$ .

The hysteresis associated with cyclic testing and the stress relaxation seen during step tests indicate that myocardium has viscoelastic properties under shear deformation. Viscoelasticity reflects energy losses due to frictional processes such as tissue fluid movement and is commonly observed in soft biological tissues (7). Viscoelasticity cannot, however, account for the history-dependent behavior seen in this study. As maximum strain was increased, stiffness decreased, and the level of stress reached at any strain was reduced. This softening was observed for maximum shear deformations of 2.5–50%, and it stabilized after one loading cycle, with no sign of recovery over periods of up to 3 h. Moreover, comparable strain softening was observed for sequential tests in *X* and *Y* directions (or vice versa)

and for shear displacement in the negative direction preceded by displacement in the positive direction, and this directional dependence is not consistent with tissue fluid shift. The reduction in passive stiffness was strain history, rather than stress, dependent: for a given maximum shear deformation, proportionately similar softening was seen in all shear modes, despite marked differences in associated stresses.

Very similar behavior has been observed in intact hearts. Emery et al. (6) recorded ventricular pressure-volume relations in isolated arrested rat hearts during cycles of LV balloon inflation and deflation. They showed that, with passive inflation to new maximum pressures, LV stiffness decreased, and they argued that this strain softening was caused by disruption of perimysial collagen due to excessive shearing between adjacent myocardial muscle layers at elevated levels of LV inflation. Our observation of shear softening at very low shear amplitudes is less readily explained in this way. There are a number of similarities between these two studies. Both used anoxic hearts that had previously been perfused with BDM to block interaction between the contractile proteins. It is possible that the softening seen at low shear amplitudes may be due to anoxia or BDM. There can be no doubt that the deformations imposed in shear testing differ from those experienced in vivo. Also, removal of test specimens would certainly have relieved residual stresses that existed in the passive LV before dissection. These factors probably contribute to the strain softening seen in this study and may explain the softening behavior at the smallest shear amplitudes. However, this phenomenon could also reflect a rearrangement of the extracellular connective tissue associated with altered mechanical loading under physiological conditions.

To make meaningful comparisons between shear properties in different directions within and between specimens, it was necessary that strain histories were carefully matched. For this reason, the same sequence of shear testing (maximum displacements of 10–50%) was imposed in each specimen for the two modes tested.

To our knowledge, this is the first investigation in which the material properties of passive ventricular myocardium have been directly characterized under shear loading. On the other hand, regional shear strain

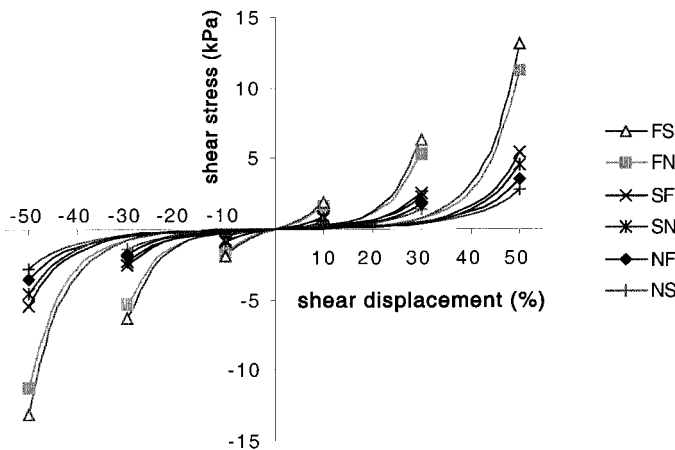


Fig. 8. Midlines of shear stress-displacement loops averaged over all 6 hearts tested. Midline data for all 6 simple shear modes were obtained from final cycle of displacement, and maximum displacement was progressively increased from 0.1 to 0.5. Midline data were fitted with a simple 3-parameter model. Mean fitted curves are presented for maximum shear displacements of 0.1, 0.3, and 0.5.

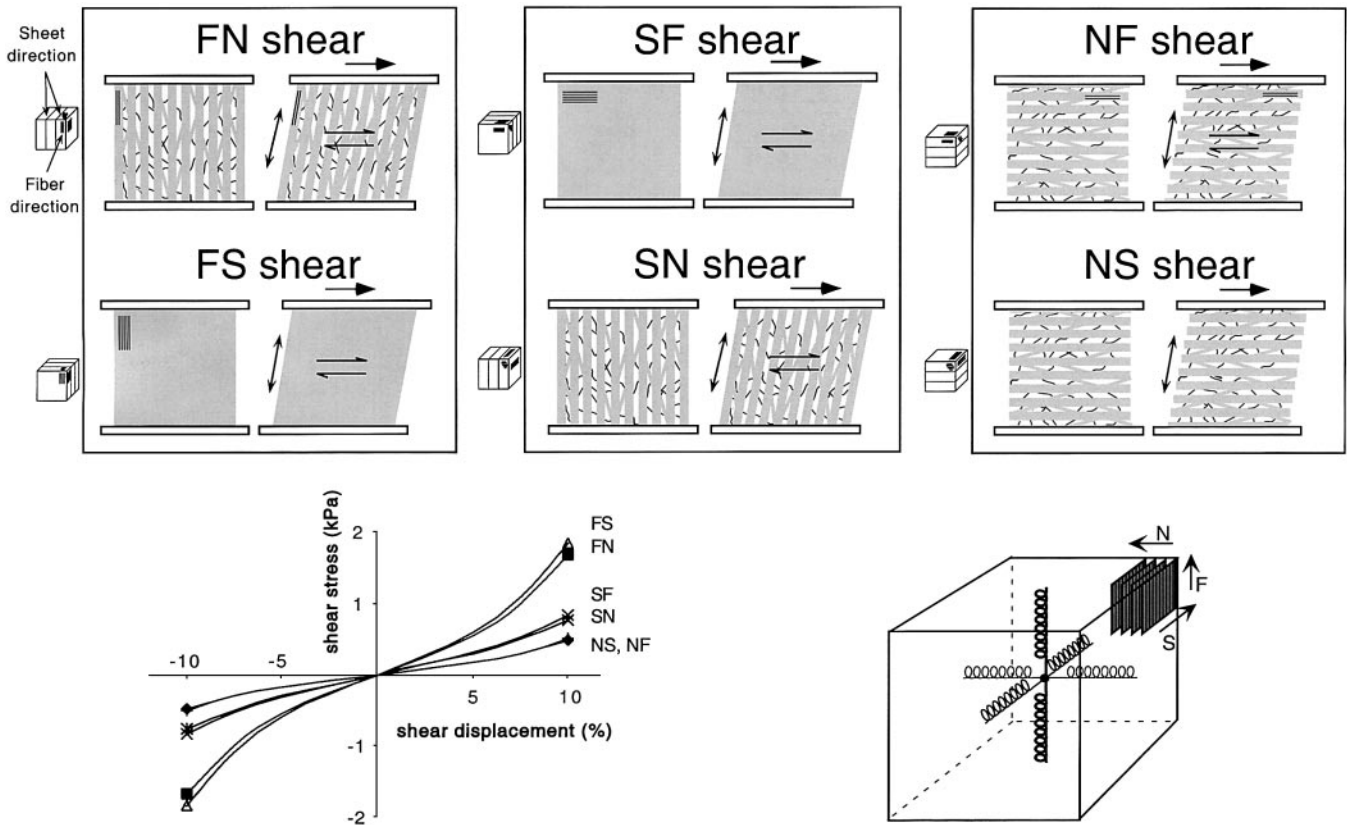


Fig. 9. Mechanical responses of passive ventricular myocardium to simple shear deformation are consistent with extension of 3 families of elastic elements, the mean orientations of which coincide with microstructurally defined axes. In undeformed state (*bottom right*), these elastic elements are aligned 1) with muscle fiber direction, 2) transverse to fiber direction in plane of sheets, and 3) normal to sheets. *Top*: deformation of these elements in 6 modes of simple shear deformation. *FN* and *FS* shear produce extension in fiber direction; *SF* and *SN* shear cause extension of elastic elements transverse to fiber direction in plane of sheets. *NF* and *NS* shear cause extension of elastic elements initially normal to sheets. *Bottom left*: mean mechanical responses for a maximum shear displacement of 0.1 from Fig. 8 on an expanded scale. Clustering of stress displacement relations for *FS* and *FN*, *SF* and *SN*, and *NS* and *NF* modes indicates that material contribution of pure shear effects is relatively small.

in the beating heart has been estimated at end systole using an end-diastolic reference state (2, 14, 25). Recent investigations of diastolic function by Takayama and co-workers (22) are directly comparable to the study presented here. Takayama and co-workers resolved end-diastolic shear strains with respect to the fiber-sheet material coordinate system used here and reported substantial shear deformation consistent with sliding displacement between adjacent layers along an axis transverse to the fibers. They showed that the extent of shear deformation at the base of the heart during filling was ordered as follows:  $SN > FN > FS$ . This indicates a progression of shear stiffness as follows:  $FS > FN > SN$ , which is consistent with our results for specimens from the same region.

The maximum shear displacements used here (10–50%) cover the range of shear deformations reported for the beating heart. Moreover, our results demonstrate clear anisotropy in response to simple shear deformation, with stiffness in *FN* and *FS* modes (predominant myocyte axis direction initially perpendicular to direction of shear displacement) markedly higher

than in the four other modes. Myocardial specimens tested in *NS* and *NF* modes (myocardial laminae parallel to top and bottom plates) exhibited very low stiffness at all levels of strain, whereas the *SF* and *SN* modes had intermediate properties. These differences are consistent with the results of Costa et al. (2). Also noteworthy is the similarity of results for *FN* and *FS* modes, for *NF* and *NS* modes, and finally for *SF* and *SN* modes.

The average behaviors presented in Figs. 7 and 8 reflect consistent differences between directions across all hearts. However, there was some variation in the absolute values of stress between hearts, as indicated by the error bars in Fig. 7. These interheart differences have a number of potential origins. For example, it is possible that the effectiveness of BDM in preventing contracture varied from heart to heart, although there was no supporting evidence for this. Specimens immersed in the bathing solution, which contained BDM, remained flaccid and exhibited no change in dimension over the duration of a typical experiment. Moreover, the material properties of control specimens tested at

intervals over 3- to 4-h periods remained surprisingly constant. A second, and more likely, possibility is interheart variation in tissue architecture and collagen density. The global coordinates of the transmural blocks from which the three adjacent specimens were cut were carefully standardized. However, we observed differences in the laminar organization of these blocks from heart to heart. In some cases, there were quite extensive regions in which intersecting layers arranged nearly perpendicular to the predominant layer direction were evident (Fig. 3). The extent to which these factors influence material properties under shear deformation remains uncertain.

Simple shear is a more complex mode of deformation than pure shear, in that it imposes tensile strain in the rotated plane in addition to shear. Our equipment was designed for simple shear testing, because this is easiest to impose. Lagrangian strain tensors are given in the APPENDIX for each of the six modes of simple shear deformation. Within this context, the similarity of the results for the pairs of modes, *FN-FS*, *NF-NS*, and *SF-SN*, provides potentially important insight into the material basis of the response to shear loading.

For instance, the strain tensors in *NF* and *NS* modes have the same diagonal term, which represents extension in the direction initially normal to the direction of displacement (i.e., normal to the muscle layers for the *NF* and *NS* modes), and differ only in the symmetrical off-diagonal shear components. There is no significant difference between stresses observed for simple shear deformations in the *NS* and *NF* modes across all hearts at any magnitude of maximum shear displacement (Fig. 8). This suggests that the mechanical behavior for *NF* and *NS* modes is dominated by the tensile response to extension of the material axis that is initially normal to the muscle layers and that the contribution of pure shear terms is relatively small. A similar analysis can be applied to the other paired modes of simple shear: *FN-FS* and *SF-SN*. The observed responses of passive ventricular myocardium to simple shear deformation are consistent with the extension of three families of elastic elements, the mean orientations of which coincide with the microstructurally defined material axes of the tissue (Fig. 9). Such a view is the basis for a recently published fiber distribution model for cardiac tissue (17).

The characteristic feature of simple shear deformation in *FS* and *FN* modes is that myocytes are extended together with perimysial collagen cords aligned with (or near parallel to) the myocyte axis. We can therefore compare stress-strain curves obtained under uniaxial tensile testing with those obtained in this study. For a 50% shear deformation in the *FN* or *FS* mode, the knee (i.e., the inflection point in the stress-strain relationship at which stiffness increases sharply) in the stress-strain relationship is at 40%, while stress rises to ~15 kPa at maximum displacement. The maximum shear displacement corresponds to a fiber axis extension of 12%. Uniaxial testing of passive trabeculae (8, 23) and

biaxial testing of passive LV myocardium (20) indicate that the knee in the tensile stress-strain relationship for the fiber axis is at ~15%, with stresses rising to 15 kPa at extensions of  $\geq 18\%$ . It follows that the material behavior of myocardium under simple shear loading in *FN* and *FS* modes is consistent with results of previous tensile testing but somewhat stiffer than those results would predict. This presumes that the reference states for shear and tensile test protocols are the same. Considerable care was taken to minimize artifact due to strain softening in this study, but this has not been done in previous tensile testing.

The techniques used in this investigation have a number of limitations. Although we immersed the specimen in an organ bath during testing, we made no attempt to oxygenate it. Instead, BDM was used to maintain the tissue in a passive state. There was no change in mechanical behavior with repeated testing over several hours, suggesting that contracture did not develop and that the structural integrity of the specimen was preserved over this period. A further limitation relates to the method of applying simple shear deformation. Our testing apparatus imposes strict boundary conditions on specimens, whereas myocardium *in situ* is not constrained to the same degree. Finally, in cutting the isolated specimens used in this study, we run the risk of compromising their structural and mechanical integrity. Although considerable effort is taken to preserve the principal structural features of ventricular myocardium, it is inevitable that the testing regimen will have some influence on measured material properties. Finally, it is necessary to acknowledge that structure was not completely uniform throughout the specimens tested. There were gradual changes in sheet orientation across each block, and small subregions were observed in which laminae were oriented orthogonal to the predominant microstructural axes. This variation will inevitably blur the true extent of the differences between material directions. Use of samples from the midwall, where structure is more uniform than in the subendocardial and subepicardial regions, helps minimize this limitation. Although the problems associated with *in vitro* mechanical testing may limit the reliability of explicit material parameter identification, the approach used here has provided important new data on the material response of passive ventricular myocardium under shear loading.

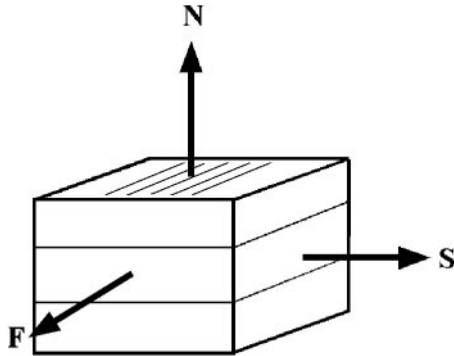
In conclusion, the results of this study suggest that the response of passive LV myocardium to simple shear deformation is dominated by the tensile material properties of the tissue along local microstructural axes and that the contribution of shear stiffness to this response is relatively small. This finding is seen to be an important step toward establishing and validating a general material law for passive ventricular myocardium. We are carrying out experiments using a wider repertoire of shear deformations to elucidate the inherent shear properties of passive cardiac tissue more fully.



APPENDIX

Strain Associated With Simple Shear Deformation

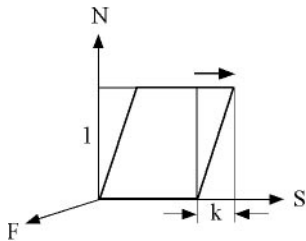
For a typical tissue specimen, the microstructural *FSN* coordinates are oriented as follows



where *F* is the myocyte axis direction, *S* lies within the muscle layer transverse to *F*, and *N* is normal to the muscle layer. Simple shear is imposed by translating one of the six faces of the cuboid while the opposite face is fixed.

There are six modes of possible shear to consider, and we will derive the Green strain tensor for the *NS* mode. We use the following conventions:  $X_1, X_2, X_3 = F, S, N$ ,  $x_1, x_2, x_3 = f, s, n$ , and *NS* shear represents translation of the *N* face in the *S* direction.

*NS mode.* A particle  $P(F, S, N)$  is deformed into  $p(f, s, n)$ . Let *k* denote the shear deformation



$$\begin{aligned} f &= F \\ s &= S + kN \\ n &= N \end{aligned}$$

The corresponding deformation gradient tensor **F** is

$$\mathbf{F} = \begin{bmatrix} 1 & 0 & 0 \\ 0 & 1 & k \\ 0 & 0 & 1 \end{bmatrix}$$

The right Cauchy-Green strain tensor **C** = *F*<sup>T</sup>*F*

$$\mathbf{C} = \begin{bmatrix} 1 & 0 & 0 \\ 0 & 1 & k \\ 0 & k & k^2 + 1 \end{bmatrix}$$

The Green strain tensor **E** is given by

$$\mathbf{E} = 0.5(\mathbf{C} - \mathbf{I})$$

Therefore, in the *NS* mode

$$\mathbf{E} = \begin{bmatrix} 0 & 0 & 0 \\ 0 & 0 & 0.5k \\ 0 & 0.5k & 0.5k^2 \end{bmatrix}$$

The right Green strain tensor is listed below for each of the remaining modes of simple shear deformation

*NF* mode

$$\mathbf{E} = \begin{bmatrix} 0 & 0 & 0.5k \\ 0 & 0 & 0 \\ 0.5k & 0 & 0.5k^2 \end{bmatrix}$$

*SN* mode

$$\mathbf{E} = \begin{bmatrix} 0 & 0 & 0 \\ 0 & 0.5k^2 & 0.5k \\ 0 & 0.5k & 0 \end{bmatrix}$$

*SF* mode

$$\mathbf{E} = \begin{bmatrix} 0 & 0.5k & 0 \\ 0.5k & 0.5k^2 & 0 \\ 0 & 0 & 0 \end{bmatrix}$$

*FN* mode

$$\mathbf{E} = \begin{bmatrix} 0.5k^2 & 0 & 0.5k \\ 0 & 0 & 0 \\ 0.5k & 0 & 0 \end{bmatrix}$$

*FS* mode

$$\mathbf{E} = \begin{bmatrix} 0.5k^2 & 0.5k & 0 \\ 0.5k & 0 & 0 \\ 0 & 0 & 0 \end{bmatrix}$$

This work was funded by the Health Research Council of New Zealand and the National Heart Foundation of New Zealand.

REFERENCES

1. **Caulfield JB and Borg TK.** The collagen network of the heart. *Lab Invest* 40: 364–372, 1979.
2. **Costa KD, Takayama Y, McCulloch AD, and Covell JW.** Lamellar fiber architecture and three-dimensional systolic mechanics in canine ventricular myocardium. *Am J Physiol Heart Circ Physiol* 276: H595–H607, 1999.
3. **Demer LL and Yin FCP.** Passive biaxial mechanical properties of isolated canine myocardium. *J Physiol* 339: 615–630, 1983.
4. **Dokos S, LeGrice IJ, Smaill BH, Kar J, and Young AA.** A triaxial-measurement shear-test device for soft biological tissues. *J Biomech Eng* 122: 471–478, 2000.
5. **Emery JL, Omens JH, Mathieu-Costello OA, and McCulloch AD.** Structural mechanisms of acute ventricular strain softening. *Int J Cardiovasc Med Sci* 1: 241–250, 1998.
6. **Emery JL, Omens JH, and McCulloch AD.** Biaxial mechanics of the passively overstretched left ventricle. *Am J Physiol Heart Circ Physiol* 272: H2299–H2305, 1997.
7. **Fung YC.** *Biomechanics: Mechanical Properties of Living Tissues.* New York: Springer-Verlag, 1993.
8. **Hanley PJ, Young AA, LeGrice IJ, Edgar SG, and Loiselle DS.** Three-dimensional configuration of perimysial collagen fibres in rat cardiac muscle at resting and extended sarcomere lengths. *J Physiol* 517: 831–837, 1999.
9. **Horowitz A, Sheinman I, Lanir Y, Perl M, and Sideman S.** Nonlinear incompressible finite element for simulating loading of cardiac tissue. I. Two-dimensional formulation for thin myocardial strips. *J Biomech Eng* 110: 57–61, 1988.

10. **Humphrey JD and Yin FCP.** Biaxial mechanical behavior of excised epicardium. *J Biomech Eng* 110: 349–351, 1988.
11. **Hunter PJ, Nash MP, and Sands GB.** Computational electro-mechanics of the heart. In: *Computational Biology of the Heart*, edited by Panfilov AV and Holden AV. Chichester, UK: Wiley, 1997, p. 416.
12. **Hunter PJ and Smaill BH.** The analysis of cardiac function: a continuum approach. *Prog Biophys Mol Biol* 52: 101–164, 1988.
13. **LeGrice IJ, Smaill BH, Chai LZ, Edgar SG, Gavin JB, and Hunter PJ.** Laminar structure of the heart: ventricular myocyte arrangement and connective tissue architecture in the dog. *Am J Physiol Heart Circ Physiol* 269: H571–H582, 1995.
14. **LeGrice IJ, Takayama Y, and Covell JW.** Transverse shear along myocardial cleavage planes provides a mechanism for normal systolic wall thickening. *Circ Res* 77: 182–193, 1995.
15. **Mulieri LA, Hasenfuss G, Ittleman F, Blanchard EM, and Alpert NR.** Protection of human left ventricular myocardium from cutting injury with 2,3-butanedione monoxime. *Circ Res* 65: 1441–1444, 1989.
16. **Nash M.** *Mechanics and Material Properties of the Heart Using an Anatomically Accurate Mathematical Model* (PhD thesis). Auckland, New Zealand: Univ. of Auckland, 1998.
17. **Nash MP and Hunter PJ.** Computational mechanics of the heart. From tissue structure to ventricular function. *J Elasticity* 61: 113–141, 2000.
18. **Robinson TF, Cohen-Gould L, and Factor SM.** Skeletal framework of mammalian heart muscle. *Lab Invest* 49: 482–498, 1983.
19. **Sacks MS.** A method for planar biaxial mechanical testing that includes in-plane shear. *J Biomech Eng* 121: 551–555, 1999.
20. **Smaill B and Hunter P.** Structure and function of the diastolic heart: material properties of passive myocardium. In: *Theory of Heart* (1st ed.), edited by Glass L, Hunter P, and McCulloch A. New York: Springer-Verlag, 1991, p. 1–29.
21. **Spotnitz HM, Spotnitz WD, Cottrell TS, Spiro D, and Sonnenblick EH.** Cellular basis for volume-related wall thickness changes in the rat left ventricle. *J Mol Cell Cardiol* 6: 317–331, 1974.
22. **Takayama Y, Costa K, and Covell J.** Contribution of laminar myofiber architecture to load-dependent changes in mechanics of LV myocardium. *Am J Physiol Heart Circ Physiol* 282: H1510–H1520, 2002.
23. **Ter Keurs HEDJ, Rijnsburger WH, van Heuningen R, and Nagelsmit MJ.** Tension development and sarcomere length in rat cardiac trabeculae: evidence of length-dependent activation. *Circ Res* 46: 703–714, 1980.
24. **Usyk T, Mazhari R, and McCulloch A.** Effect of laminar orthotropic myofiber architecture on regional stress and strain in the canine left ventricle. *J Elasticity* 61: 143–164, 2000.
25. **Waldman LK, Fung YC, and Covell JW.** Transmural myocardial deformation in the canine left ventricle: normal in vivo three-dimensional finite strains. *Circ Res* 57: 152–163, 1985.
26. **Young AA, LeGrice IJ, Young MA, and Smaill BH.** Extended confocal microscopy of myocardial laminae and collagen network. *J Microsc* 192: 139–150, 1998.

